JOURNAL OF AIRCRAFT
Vol. 42, No. 6, November–December 2005

Flutter Analysis for the F-16A/B in Heavy Store Configuration

Samir Bennani*
Delft University of Technology, Kluyverweg 1, 2629 HS, Delft, The Netherlands
Bert Beuker†
Royal Netherlands National Air Force, Binkhorstlaan 135, 2516 BA, The Hague, The Netherlands
Jan Willem van Staveren‡
ADSE Consultancy and Engineering Services, Saturnusstraat 12, 2130 KB, Hoofddorp, The Netherlands
and
Jos J. Meijer§
National Aerospace Research Laboratory, Anthony Fokkerweg 2, 1059 CM, Amsterdam, The Netherlands

This work compares Several analytical approaches are compared for in-flight flutter margin calculations for an F-16A/B in heavy store configuration. Nominal flutter model formulations are developed in terms of the dynamic pressure and the Mach number. These analysis models are expressed within the linear fractional transformation (LFT) framework for the determination of flutter onset conditions using the structured singular value μ analysis. The results obtained from classical analysis tools such as the P and P–K method, as well as the μ method are compared with each other and validated using actual flight-test data. The LFT model parameterization in terms of match-point Mach number is novel and permits a natural and efficient flight-test procedure for flutter envelope clearance. Structural parameter variations such as changes in wing mass, as well uncertainties in damping and/or stiffness, are also incorporated in the LFT formulation and permit the calculation of robust match-point flutter margins. The μ-analysis results obtained from such model formulations incorporating several simultaneous parameter variations reveal and explain the complex physical mechanisms that have led to limit-cycle oscillation conditions encountered during the flight tests.

Nomenclature

A_i	=	approximation coefficient matrix
b	=	reference span
f	=	frequency
K	=	stiffness matrix
k	=	reduced frequency
M	=	mass matrix
Ma	=	Mach number
Ma_{flutter}	=	flutter Mach number
Ma_{mo}	=	maximum operating Mach number
n	=	number aerodynamic lag modes
P	=	set of system operators
p	=	roll rate
Q	=	aerodynamic coefficient matrix
$\tilde{Q}$	=	approximation of Q
q	=	dynamic pressure
q_{flutter}	=	dynamic flutter pressure
r	=	yaw rate
$S(\omega)$	=	power spectral density
s	=	Laplace operator
V	=	velocity
V_{flutter}	=	flutter velocity
V_{mo}	=	maximum operating speed
V_s	=	speed of sound
x	=	aerodynamic states
β	=	angle of side slip
β_i	=	aerodynamic lag terms
η	=	generalized coordinate
μ	=	structured singular value
ρ	=	density
ω	=	frequency

Presented as Paper 2002-3967 at the AIAA 36th Guidance, Navigation and Control Conference, Monterey, CA, 5–8 August 2002; received 30 December 2003; revision received 14 February 2005; accepted for publication 14 February 2005.

*Assistant Professor, Control and Simulation Division, Delft Aerospace, Kluyverweg 1. Member AIAA.
†Senior Research Engineer.
‡Research Engineer.
§Senior Research Engineer, Department of Flight Physics and Loads. Member AIAA.

Introduction

RECENTLY NASA[1,2] has reported some promising advances in the field of model-based in-flight structural mode and flutter analyses. Especially, the development of an on-line model-based flight flutter prediction concept, the so-called flutterometer,[3–9] has great potential in contributing to more efficient flight envelope clearance procedures.

Flutter,[10] which reflects an aeroelastic instability, occurs at a particular flight condition where the structural mode damping vanishes. This condition of instability, mostly characterized in terms of airspeed, dynamic pressure, or the Mach number, pinpoints one single flight envelope boundary condition. It has been reported[11–15] that clearing the full flutter envelope point for point can be a dangerous, labor intensive, and expensive process. In conjunction with these flight tests, mainly traditional analytical nominal flutter prediction methods are used, such as the P, the K, and the PK method.[15] Besides predicting only a nominal flutter condition, corrections for the free air density parameter must be performed to provide a match-point flutter solution. Furthermore, when working in experimental conditions, the traditional methods need to be handled with great care. This is especially the case when, during flight tests, potentially explosive flutter conditons are approached. In the vicinity of such conditions, the gradient in the system damping is very steep and can lead to severe structural damage. To overcome these drawbacks, safer, more versatile, and more efficient flutter prediction methods have been recently proposed.[3,16–19]

In contrast to the traditional methods, the new techniques have the predicate robust. The term robust is motivated by the fact that one accounts for potential model errors between the physical system and some reference structural dynamics. These model errors

can be determined online using advanced excitation, filtering, and identification techniques.[6,9,20–23]

In this paper, the initial formulation of the flutter analysis model is similar to that presented in Refs. 3 and 24. It relies on a single parameter linear fractional representation (LFR) of the aeroelastic equations of motion. The parameterization is given in terms of a varying dynamic pressure. The stability of the linear fractional transformation (LFT) model with respect to dynamic pressure deviations from a nominal condition is determined using the structured singular value μ as developed by Packard and Doyle.[25] The μ analysis is a general tool for the determination of the worst-case stability condition in a system subjected to a set of simultaneous perturbations with a predefined structure. A more in-depth treatment of the subject can be found in Refs. 3 and 26 and references therein. Numerical reliable tools efficiently implementing the μ theorem are readily available in commercial software packages[26] running under MATLAB®. In the context of robust flutter margin determination, the concept of a structured perturbation model is used to reflect changes in flight condition (airspeed, dynamics pressure, Mach, and air density) together with potentially expected uncertainties in the system's mass, damping, and stiffness. Remodeling such system variations into an LFR can be performed using various numerical and analytical techniques. An overview of the LFT modeling procedures applied to complex aerospace systems has been recently reported in an extensive study dedicated to the clearance of flight control systems.[27] From this same research, reliable numerical tools[28] along with the initial concept of Lambrechts et al.[29] have been developed for the automatic generation of complex LFT models. At NASA Langley Research Center, similar research efforts are conducted in the context of a National Aviation Safety Program.[30,31]

In this work, a series of aeroelastic analysis models is developed for the determination of nominal as well as robust flutter conditions. It is shown that in the nominal case the single parameter LFT coincides with the traditional P and PK formulation. The initial nominal single parameter LFT models are developed in terms of dynamic pressure variation using an analytical approach[3] as well as numerical LFT generation tools.[28] The obtained LFT formulations are validated by comparing the results from the μ analyses and the classical P and PK method with measured limit-cycle oscillation (LCO) conditions resulting from flight-test runs. The initial flutter analyses of the F-16A/B fighter aircraft located aeroelastic problems in heavy underwing store configuration. The problems revealed as LCOs of the wing tips. Measured wing tip accelerations during accelerated Mach maneuvers as shown in Fig. 1 are used to compare the analytical flutter results.

Several authors[32–34] have pointed out that the LFT formulation in terms of dynamic pressure fails in delivering match-point flutter speeds. Reformulating the LFT model in terms of airspeed[32] or in terms the Mach number variations [33,34] provide direct ways to obtain match-point solutions while greatly enhancing and simplifying the flutter clearance flight-test procedure.

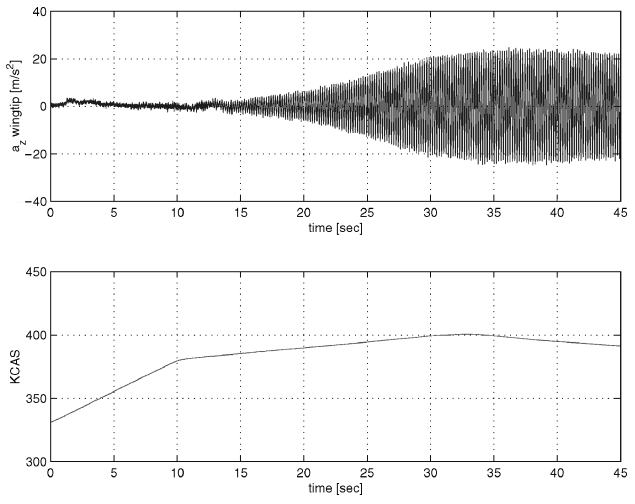

Fig. 1 Measured wing tip acceleration in level accelerated flight.

In this paper, we present the LFT modeling principles for the match-point Mach formulation. Again μ-analysis results are compared with measurements obtained from flight tests. To reflect the fuel consumption of the wing pylon tanks, the single parameter Mach-dependent LFT model is refined through augmentation with a mass perturbation parameter. Previous studies as well as flight tests have shown that pylon fuel contents greatly affects the wing tip LCO behavior. It was not exactly understood how the LCO behavior evolved as a function simultaneous mass and Mach variations. The full fuel tank contents is 2600 lb per tank and can be sequentially drained down to empty. There are three fuel compartments in the wing pylon tank, and a low-cost design change to resequence the wing pylon fuel consumption has been carried out to alleviate the LCO problem after flight flutter testing.[35]

The fuel drain sequence from full, indicated as full–full–full (FFF), starts by using only the midcompartment. In the half-full fuel state, indicated as full–empty–full (FEF), the forward and aft compartments are drained simultaneously. After that, fuel is used from the aft compartment. In the quarter-full fuel state, indicated as full–empty–empty (FEE), only the forward compartment contains fuel and is drained until the tank is empty indicated as empty–empty–empty (EEE). Obviously such a fuel sequence causes an irregular change of the center of gravity of the fuel tank, resulting in a nonlinear change of the moment of inertia of the wing with respect to changes in the fuel state. The modeling of the fuel state in the wing pylon fuel tank was divided into four sequences, the FFF, FEF, FEE, and EEE states. Accordingly one single LFT model is developed covering the fuel state sequences as a function of the flight condition. Parameter-dependent μ analyses lead to a series of match-point fuel state-dependent Mach flutter speeds, which are compared with LCO wing tip acceleration data obtained from flight-test runs. To conclude the work, some robust match-point Mach flutter margins are developed to illustrate the effect of uncertain damping and stiffness coeffcients.

Aeroelastic Dynamics Modeling

Flutter analysis relies on the solution of the equation of motion for structural aircraft response, which at a constant Mach number is given as

$$M\eta s^2 + C\eta s + K\eta = qQ(s)\eta \tag{1}$$

with M, C, and K the generalized mass, damping, and stiffness matrices. The term $q = 1/2\rho V^2$ is the dynamic pressure at which the system is considered. The unsteady aerodynamic forces acting on the right-hand side of the system (1) are determined in terms of a frequency-dependent matrix $Q(k, Ma)$. These forces are obtained using the doublet-lattice method (DLM) incorporated in the NASTRAN software package.[36,37] The DLM method is applicable up to subsonic airflows for Mach numbers not larger than $Ma = 0.8$. With the speed of sound V_s, the Mach number is defined as $Ma = V/V_s$. With the reduced frequency k defined as $k = \omega b/2V$, the antisymmetric modes depend on the radial frequency ω, the wing span b, and the true airspeed V. The radial frequency ω belongs to a certain mode shape, and the coefficients in the matrix Q reflect the aerodynamic influence between the different mode shapes at the matching reduced frequency k_i. A finite element method (FEM) model of the F-16A/B with heavy underwing stores as shown in Fig. 2 is developed within NASTRAN. To determine the structural mode shapes, the unforced equations of motion are solved,

$$M\eta s^2 + C\eta s + K\eta = 0 \tag{2}$$

within NASTRAN.

The analysis indicates an aerodynamic coupling between antisymmetric structural modes (structure-to-structure aerodynamic coupling). The modes with the strongest influence on the LCO phenomena were the antisymmetric wing tip pitch and plunge and the antisymmetric pylon tank on wing stations 4 and 6 (wing tip) pitch mode. The influence of the last mode decays with decreasing fuel quantity in the wing pylon tanks. With this knowledge, the antisymmetric rigid-body modes and a limited number of antisymmetric structural mode shapes were taken into account in the mode shape

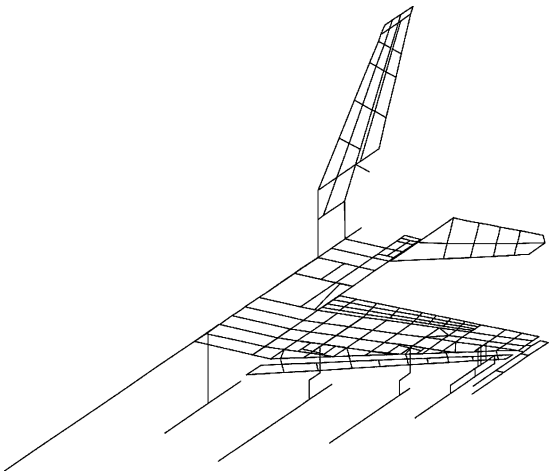

Fig. 2 F-16 finite element model.

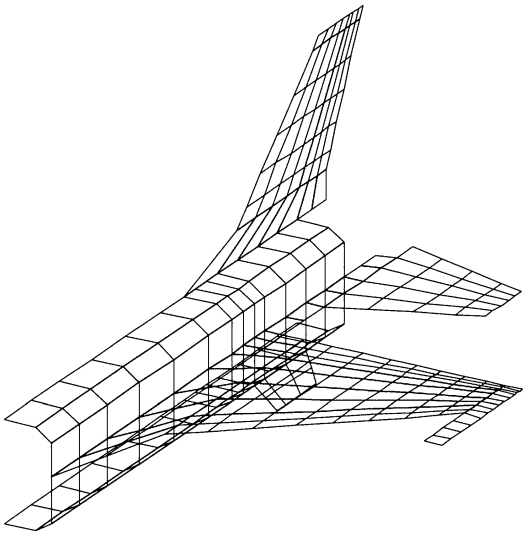

Fig. 3 F-16 doublet lattice panel layout.

analysis. The aerodynamic contribution is calculated on the basis of the DLM method, producing values for the unsteady aerodynamic coefficients $Q(s)$. This method assumes compressible, inviscid, and irrotational airflows and requires a discrete approximation of the aircraft's lifting surfaces and fuselage in the form of panels. The panel layout is detailed in Fig. 3.

The method produces the coefficients of $Q(k, Ma)$ as a function of reduced frequency k and Mach number Ma. The aerodynamic coefficients were calculated at a discrete selection of reduced frequencies and Mach numbers. Taking the frequency of the structural modes and the airpseed range at sea level into account, the reduced frequencies were selected from 0.0001 to 1.5 with increments of 0.1 and the Mach numbers between 0.4 and 0.8 with increments of 0.05. The unsteady aerodynamic forces $Q(k, Ma)$ are a function of the reduced frequency k and can, therefore, be represented by the frequency domain. To apply the P method for the flutter analysis, the coefficients of $Q(k, Ma)$ have to be transformed into the time domain by means of a rational function approximation.

Aerodynamic Coefficients Approximation

We use the so-called Padé function approximation (see Ref. 38) to obtain the transfer function matrix,

$$\bar{Q}(s)\eta = \left[A_0 + A_1 s\frac{b}{2V} + A_2 s^2\left(\frac{b}{2V}\right)^2 + \sum_{n=1}^{N} A_{2+n}\frac{s}{s+\beta_n(2V/b)}\right]\eta \tag{3}$$

Expressing the aerodynamic forces in this way is referred to as Roger's formulation.[12] Furthermore, each aerodynamic lag term is defined as a new state,

$$x_n = \{s/[s+\beta_n(2V/b)]\}\eta \tag{4}$$

The obtained aerodynmic formulation includes pairs of aerodynamic lag terms with a common denominator. The lag terms are high-pass filters with break frequencies dictated by the coefficients β_{n_1} and β_{n_2}. The choice of β_{n_1} and β_{n_2} is restricted to be real and positive to ensure the system's stability. At each selected Mach number, the coefficients A_i and $b/2V$ are interpolated as a function of the reduced frequency k using the relationship between the antisymmetric reduced frequencies,

$$k = \omega b/2V \Rightarrow jk = j\omega b/2V \tag{5}$$

$$s = j\omega \Rightarrow jk = s(b/2V) \tag{6}$$

Approximation in the Linear Time Invariant Framework

A state-space realization of the lag terms and inclusion of these terms in the generalized equation of motion is proposed in Ref. 39. Implementing the lag terms into the generalized equation of motion generates, besides the rigid-body and structural modes η, aerodynamic modes x_n. Details concerning the derivation of the equations developed are outlined in Appendix A of Ref. 33. The resulting set of differential equations is given by

$$\begin{bmatrix}\dot{\eta}\\ \ddot{\eta}\\ \dot{x}_1\\ \vdots\\ \dot{x}_n\end{bmatrix} = \begin{bmatrix}0 & I & 0 & \cdots & 0\\ -\bar{M}^{-1}\bar{K} & -\bar{M}^{-1}\bar{C} & \bar{M}^{-1}A_3 q & \cdots & \bar{M}^{-1}A_{2+n}q\\ 0 & I & -B_1 & \cdots & 0\\ \vdots & \vdots & \vdots & \ddots & \vdots\\ 0 & I & 0 & \cdots & -B_n\end{bmatrix} \times \begin{bmatrix}\eta\\ \dot{\eta}\\ x_1\\ \vdots\\ x_n\end{bmatrix} \tag{7}$$

where

$$B_n = \left(\frac{b}{2V}\right)\begin{bmatrix}\beta_n & 0 & 0\\ 0 & \ddots & 0\\ 0 & 0 & \beta_n\end{bmatrix} \tag{8}$$

with $\bar{M}$, $\bar{C}$, and $\bar{K}$ defined as

$$\bar{M} = M - A_2(b/2V)^2 q \tag{9}$$

$$\bar{C} = C - A_1(b/2V)q \tag{10}$$

$$\bar{K} = K - A_0 q \tag{11}$$

The set of differential equations forms the basis for the analysis of the desired linear time invariant (LTI) system. Flight control laws might be added to the LTI system leading to additional states and/or feedback loops. In this paper, the flight control laws were not added to the LTI system. Notice that the coefficients of the matrices A_i interpolated as a function of the reduced frequency k are also Mach dependent.

Matched and Unmatched Flutter Solutions

Based on the system dynamics (7), flutter analysis is performed at selected Mach numbers by scaling the dynamic pressure q for a fixed altitude. The dynamic pressure q for which one of the structural modes becomes unstable is indicated as the dynamic flutter pressure q_{flutter}. The dynamic flutter pressure q_{flutter} can also be expressed in terms of a flutter speed V_{flutter} or a flutter Mach number Ma_{flutter} by

taking into account the selected altitude in terms of the air density and/or speed of sound. The result is an unmatched flutter solution because the selected Mach number is not likely to be the same as the flutter Mach number. Flutter analysis has to be performed again taking the earlier found flutter Mach number as a new initial condition for the selected Mach number. The process is performed iteratively until the selected Mach number matches the flutter Mach number. When the selected and the flutter Mach number are equal, the flutter solution is called a match-point flutter solution.

Calculating Flutter Margins

The generalized equation of motion for the structural response is now expressed in a form that is suitable to compute the flutter margin (see Ref. 3). The flutter margin is dependent on the flight condition parameter that results in flutter instability.

For flutter analysis, the flight condition parameter is perturbed to find the smallest perturbation that causes an instability. From the LTI representation, it is clear that the unsteady aerodynamic forces are scaled by the dynamic pressure q at a constant Mach number. Perturbations in dynamic pressure can, thus, enter the system through a feedback operator in a linear fractional manner that is suited flutter analysis. The dynamic pressure is perturbed from nominal q_0 with an additive uncertainty δ,

$$q = q_0 + \delta q \tag{12}$$

By defining the signal z as an output of the nominal system P,

$$z = P(q_0)w \tag{13}$$

and defining the perturbation operator δq as

$$w = \delta q z \tag{14}$$

we obtain the desired LFT model in state-space form

$$\begin{bmatrix} \dot{\eta} \\ \ddot{\eta} \\ \dot{x}_1 \\ \vdots \\ \dot{x}_n \\ z \end{bmatrix} = \left[\begin{array}{ccccc|c} 0 & I & 0 & \cdots & 0 & 0 \\ -\bar{M}^{-1}\bar{K} & -\bar{M}^{-1}\bar{C} & \bar{M}^{-1}A_3 q_0 & \cdots & \bar{M}^{-1}A_n q_0 & I \\ 0 & I & -B_1 & \cdots & 0 & 0 \\ \vdots & \vdots & \vdots & \ddots & \vdots & \vdots \\ 0 & I & 0 & \cdots & -B_n & 0 \\ \hline P1 & P2 & P3_1 & \cdots & P3_n & P4 \end{array}\right] \times \begin{bmatrix} \eta \\ \dot{\eta} \\ x_1 \\ \vdots \\ x_n \\ w \end{bmatrix} \tag{15}$$

where the elements of the output and feedthrough matrices are defined as

$$P1 = -(\bar{M}^{-1})^2 A_2 \left(\frac{b}{2V}\right)^2 \bar{K} + \bar{M}^{-1}A_0 \tag{16}$$

$$P2 = -(\bar{M}^{-1})^2 A_2 \left(\frac{b}{2V}\right)^2 \bar{C} + \bar{M}^{-1}A_1 \frac{b}{2V} \tag{17}$$

$$P3_n = (\bar{M}^{-1})^2 A_2 \left(\frac{b}{2V}\right)^2 \left[\sum_{n=1}^{N} A_{2+n}\right] q_0 + \bar{M}^{-1}\left[\sum_{n=1}^{N} A_{2+n}\right] \tag{18}$$

$$P4 = \bar{M}^{-1}A_2 \left(\frac{b}{2V}\right)^2 \tag{19}$$

Generation of the LFT model was performed by reformulating the generalized equation of motion for structural response with the perturbation in dynamic pressure. The LFT model was generated analytically as well as numerically by using the LFR Toolbox.[28] With the LFT model, the flutter margin is calculated at a selected Mach number; therefore, the flutter margin expressed in dynamic pressure is still an unmatched flutter solution.

Flutter Margin with Mach Perturbation

As mentioned, perturbation of the dynamic pressure leads to an unmatched flutter solution. For flight-test purposes, it is desirable to obtain matched flutter solutions. To identify a suitable flight condition parameter for perturbation, one should consider flight flutter test procedures. The most common procedure is the level acceleration. At a certain flight level, the run is started at a minimum speed, for instance, at $1.2V_{\min}$. The acceleration is controlled with engine power, while maintaining level flight. The run is terminated at a predetermined speed, a maximum airspeed V_{mo}, or a maximum Mach number Ma_{mo}. To perform these tests in a safe manner, flight-test crews must be provided with adequate limitations in terms of flutter speed. From the way these tests are executed, it is clear that these limitations must be matched flutter solutions. For the LFT model, a constant altitude implicates that the altitude and, thus, air density and the speed of sound at that particular flight level are fixed. All of the flight condition variations can now be expressed as a function of Mach number only. In Ref. 16, it is also recommended to relate variations in all aerodynamic coefficient derivatives to variations in Mach number. The flutter margin is expressed as a Mach number margin valid at the considered flight level. The Mach number is perturbed from nominal Ma_0 with an additive uncertainty δMa,

$$Ma = Ma_0 + \delta Ma \tag{20}$$

To obtain the desired LFT model reflecting the Mach number dependence, define the output signal z as

$$z = P(Ma_0)w \tag{21}$$

and the feedback signal w as

$$w = \delta Ma z \tag{22}$$

The coefficients of the A_i matrices are all a function of Mach. A fit of the coefficients of all matrices was performed using a second-order fit in Mach number. Moreover, the factor $b/2V$ and the dynamic pressure q also must be expressed as a function of Mach. Reformulating the generalized equation of motion for structural response with a Mach perturbation only leads to a nonlinear equation of motion in powers of Mach up to Ma^4; for details, refer to Appendix C in Ref. 33. It is not straightforward to obtain a Mach parameterized LFT model in a literal fashion using analytic manipulations; instead of that, we obtained the desired LFT model numerically by using symbolic matrix manipulations coded within the LFR Toolbox.[28] These matrix coefficients are approximated using a second-order polynomial fit in the Mach number,

$$A_i(Ma) = A_i\left(m_2 Ma^2 + m_1 Ma + m_0\right) \tag{23}$$

Expressing the matrices $\bar{M}$, $\bar{C}$, and $\bar{K}$ in terms of the Mach number leads to

$$\begin{aligned} \bar{M} &= M - A_2(b/2V)^2 q \\ &= M - \left(b^2/4Ma^2V_s^2\right)\left(\rho Ma^2 V_s^2/2\right)A_2(Ma) \end{aligned} \tag{24}$$

with

$$A_2(Ma) = A_2\left(m_2 Ma^2 + m_1 Ma + m_0\right) \tag{25}$$

$$\begin{aligned} \bar{C} &= C - A_1(b/2V)q \\ &= C - (b/2MaV_s)\left(\rho Ma^2 V_s^2/2\right)A_1(Ma) \end{aligned} \tag{26}$$

with

$$A_1(Ma) = A_1\left(m_2 Ma^2 + m_1 Ma + m_0\right) \tag{27}$$

$$\bar{K} = K - A_0 q$$

$$= K - \left(\rho Ma^2 V_s^2 / 2\right) A_0(Ma) \tag{28}$$

with

$$A_0(Ma) = A_0\left(m_2 Ma^2 + m_1 Ma + m_0\right) \tag{29}$$

All coefficients of Eq. (7) are now expressed as a function of Mach and correspond to a certain altitude fixing the air density ρ and the speed of sound V_s to constant values. The advantage of the described method is that the matched flight flutter condition is obtained solving an eigenvalue problem for Eq. (7) without any iteration process. The difficulty in the method lies in the extensive curve fitting of the coefficients of $Q(k, Ma)$ to obtain polynomial expressions in the Mach number. In this way, the resulting Mach-dependent state-space equation is automatically reformulated in an LFT format suitable for robustness analysis.

Nominal Analysis Results

First we present the NASTRAN mode shape analysis results obtained based on the FEM model shown in Fig. 2. To validate the approximation of the unsteady aerodynamic coefficients, the results of the P method are compared with the PK method. Then flutter margin calculation obtained from the P method are compared with results from both the analytically obtained LFT model and the numerically obtained LFT model. Both LFT models consider a variation in the dynamic pressure. Next, we compare the flutter analysis results for a generated LFT model depending on the Mach number. The results of the P method are compared with the results of the numerically obtained Mach parameterized LFT model. Finally, the so obtained analytical predictions are compared with LCO conditions encountered during flight tests.

Structural Mode Shape Analysis

The FEM model was configured in the heavy underwing store configuration with grid point restraints set to allow antisymmetric structural modes. The nominal fuel mass distribution of the model was adjusted to match the flight-test conditions as closely as possible, leading to a configuration with partially filled wing pylon tanks. In the analysis, four structural modes were considered; these are shown in Fig. 4.

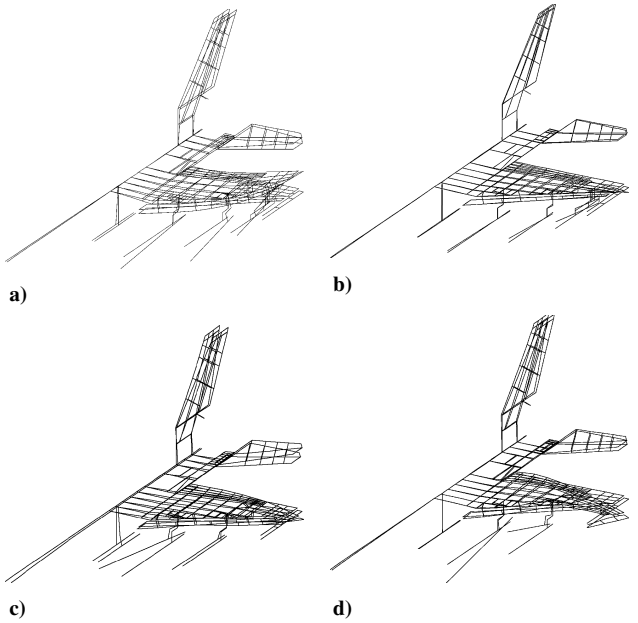

Fig. 4 F-16 mode shapes: a) wing bending mode 4.93 Hz, b) wing torsion mode 5.35 Hz, c) PT yaw mode 7.22 Hz, and d) PT pitch mode 7.52 Hz.

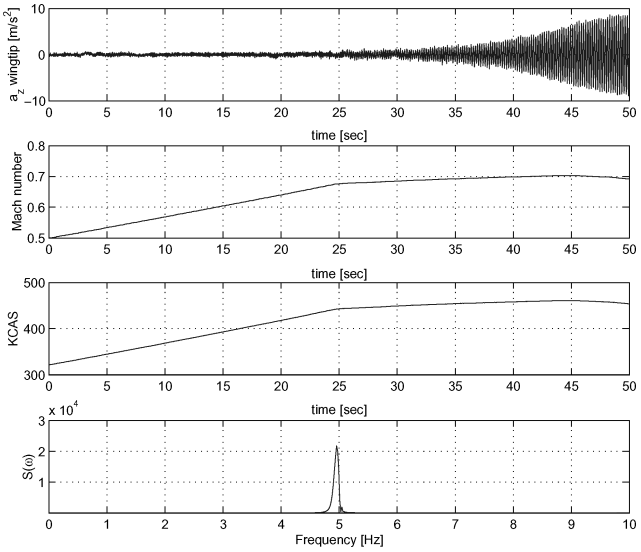

Fig. 5 Flight-test results for level acceleration at 1000 ft.

Figure 4a shows the first structural mode shape $\eta_1 = 4.93$ Hz, which reflects the wing tip bending mode. The second mode η_2 at 5.35 Hz shown in Fig. 4b is the first wing torsion mode. The pylon fuel tank twist mode η_3 at 7.2 Hz is shown in Fig. 4c. Finally, Fig. 4d shows the wing tip fuel tank pitch mode η_4, which is at a frequency of 7.52 Hz.

Nominal LCO Flight-Test Results

The flight-test results are obtained with a level acceleration at 1000-ft above ground level (AGL) above the North Sea with a low sea state and calm air. The run was performed in a heavy store configuration with partially filled wing pylon tanks at wing stations, 4 and 6 (nominal mass condition). The results of the test run are shown in Fig. 5. The wing tip normal acceleration a_z (in meters per second squared) is measured at the tip of the missile launcher. Figure 5 indicates the onset of LCO at about 30 s from the start of the accelerated run. This corresponds with an airspeed of 450 knots calibrated airspeed (KCAS) and a Mach number of 0.68 as indicated by the two middle parts in Fig. 5. The bottom trace in Fig. 5 shows the Fourier transform of the wing tip normal acceleration. The peak value of the power spectral density function $S(\omega)$ occurs at a frequency just below 5 Hz. The exact frequency corresponds to the wing tip plunge mode $\eta_1 = 4.93$ Hz as deduced by the earlier modal analysis.

Comparison of the PK and P Methods

To obtain matched flutter solutions, results of both the PK and the P methods are produced at various Mach numbers. The selected Mach numbers are varied from 0.4 to 0.8 with step size 0.05, whereas the selected reduced frequencies range from 0.0001 to 1.5 with increments of 0.1. The results of the PK method produced using NASTRAN are in Fig. 6. The results of the P method, shown in Fig. 7, were generated by calculating within NASTRAN the Q matrix at selected reduced frequencies and Mach numbers. The fitting of the Q matrix and the solution of the generalized equation of motion was performed using MATLAB routines. In Table 1, the results are summarized. The difference between the results of the PK and the P method is about $\frac{1}{2}\%$ maximum. The fitting of the Q matrix might be the cause of the difference between the methods. To obtain a matched flutter solution, we calculate the flutter Mach number of the PK solution at sea level with a selected Mach number of 0.7, and we find 0.696. The selected Mach number and the flutter Mach number are very close, that is, the matched flutter speed V_{flutter} is very near 462 knots equivalent airspeed (KEAS) and Ma_{flutter} is very near 0.7 at sea level. The difference between the analytical flutter solutions

Table 1 PK- and P-method results at sea level

Selected Mach	PK method V_{flutter}, KEAS	P method V_{flutter}, KEAS	Flight test V_{LCO}, KCAS/Ma
0.6	473	473	
0.7	462	462	
0.8	446	448	
			450/0.68

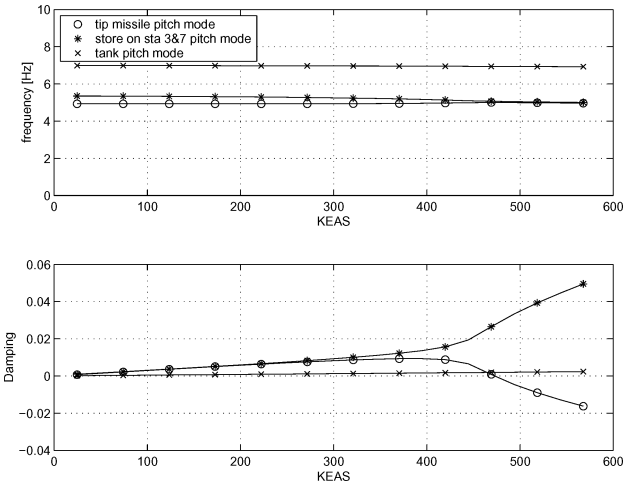

Fig. 6 Frequency and damping PK method for Mach = 0.6.

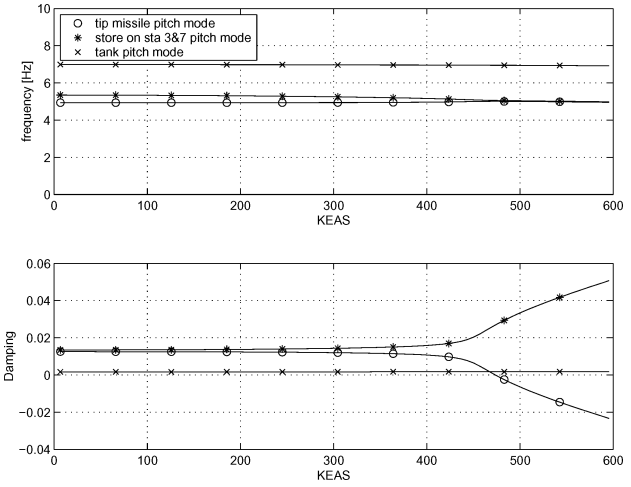

Fig. 7 Frequency and damping P method for Mach = 0.6.

and the flight-test results might be explained by possible difference in modeled mass and actual aircraft mass due to fuel burn during the level acceleration and possible inaccuracies in structural damping of the FEM model. The analytical results obtained are reasonable because they are within a 5% margin of the flight-test results. The frequency and damping curves of both methods (Figs. 6 and 7) show the frequencies of the first three structural modes. The frequencies of the first two modes, the wing tip pitch and plunge mode, converge with increasing airspeed. The damping of the first mode increases and the damping of the second mode decreases with increasing airspeed. Eventually, the damping of the second mode crosses the zero axis, indicating that the mode becomes unstable (negative damping). The point on the airspeed axis were the damping vanishes is called the flutter speed. The unstable mode is confirmed by the fight-test data that reveal an LCO of the wing tip pitch mode at Mach 0.68. One might argue that in the analysis accounting only for four structural mode shapes is rather minimal. To verify the results, the PK method was also performed taking into account structural mode shapes up to 42 Hz. No significant influence on the flutter speed was noticed. Apparently, the flutter mechanism of the first four structural modes dominates and is barely influenced by structural modes with higher frequencies. However, we are aware that it is by no means a standard procedure in flutter analysis to account for such a low number of structural modes.

Table 2 Comparison flutter tests

Model	Result
P method	
q_{flutter}	5.268
Ma_{flutter}	0.7
Analytical LFT	
q_{flutter}	5.211
Ma_{flutter}	——
Numerical LFT	
q_{flutter}	5.412
Ma_{flutter}	0.698
Flight test	
q_{LCO}	4.761
Ma_{LCO}	0.68

Results: P Method, Analytical, and Numerical LFT with Dynamic Pressure Perturbed

The Mach number range that was used for the calculation of the dynamic flutter pressure with the P method is from 0.4 to 0.8 at sea level. The comparison between the models was made at Mach 0.6, which is in the center the range. In the LFT model, this corresponds to the unperturbed nominal Mach number $Ma_0 = 0.6$. The selected Mach number for using the P method was also at 0.6. From the flutter speed obtained with the P method (473 KEAS), the dynamic pressure, at sea level, was calculated. Also, from the LCO onset speed obtained during the flight test (450 KCAS), the dynamic pressure, at 1000-ft AGL, was calculated. Table 2 summarizes the dynamic flutter pressure analysis results (in pounds per square inch) obtained from the P method, the analytical LFT model, and the numerical LFT. These computed results are compared with the LCO condition obtained from flight tests.

The analysis results show very close correlation between the P method, the analytically obtained LFT model, and the numerically obtained LFT model. The difference between the results from the P method and the analytical LFT model originate from the factor $b/2V$. In the analytical LFT model, this factor has been kept constant around the nominal flutter pressure. The discrepancy in the analysis results between both LFT models comes from the fact that we did not take into account the dynamic pressure perturbation in the apparent mass term [Eq. (24)]

$$\left[M - A_2(q_0 + \delta q)(b/2V)^2\right]\ddot{\eta} \tag{30}$$

which means that the term δq in Eq. (30) is set to zero.

The reason why this part of the dynamic pressure perturbation has not been taken into account in the numerical uncertainty modeling is twofold. First, this term has a relative marginal contribution to the flutter pressure when comparing the result from the P method. From a practical modeling consideration, the apparent mass term (30) does enter the LFT model in an inverse fashion, complicating the modeling effort while negatively affecting the numerical reliability of the model. The lower LCO onset from the flight test can be explained by the smaller flutter speed at 1000-ft AGL, where air density is lower than at sea level.

Results: P Method, Numerical LFT with Mach Perturbation

The generalized equation of motion for structural response is reformulated with the Mach number as a varying parameter for the determination of the flight condition at which the Mach flutter speed occurs. At constant altitudes the values for the air density and the speed of sound are fixed. The matched flutter solution is only valid at the selected altitude. In our case, we consider the altitude to be at sea level for a range of Mach numbers varying from 0.4 to 0.8. When the P method is applied for the determination of matched Mach flutter solutions, the stability of the structural modes

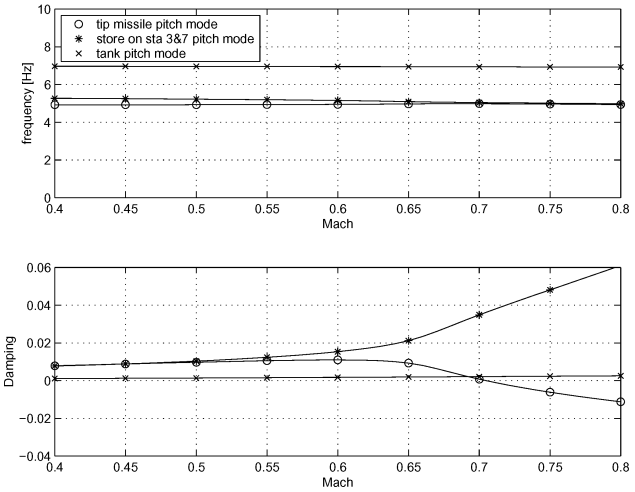

Fig. 8 Frequency and damping P method, Mach fitted, sea level.

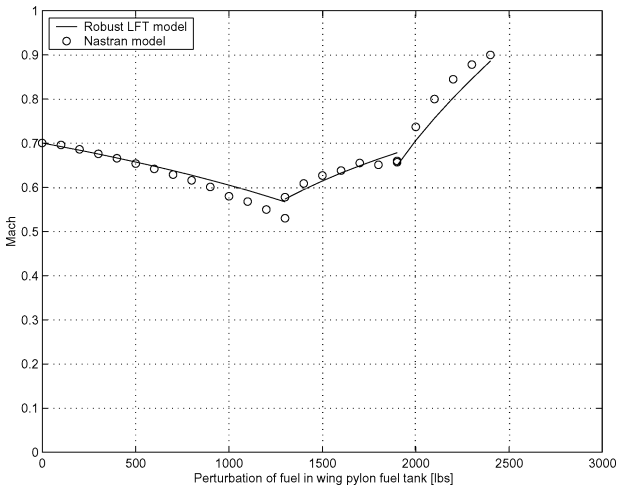

Fig. 9 Flutter analysis with mass perturbation, FFF to EEE.

is evaluated over the considered range of Mach numbers. From this evaluation, the frequency and damping curves are obtained as shown in Fig. 8. To be able to calculate matched Mach flutter margins, one must develop a Mach-dependent LFT model for which the Mach perturbation parameter is made explicit. Because of the complex dependence of the elements of the generalized equation of motion on the Mach number, the generation of the Mach-dependent LFT model was performed using dedicated numerical tools.[28]

A comparison between the methods was made for a nominal Mach number of 0.6. The outcome of the P method is presented in Fig. 8. In Table 2, all results are summarized.

From Fig. 8, it is clear that the frequency and damping curves show the same behavior as the P-method with airspeed or dynamic pressure as flight condition parameter. The main advantage for using the Mach number as the varying flight condition parameter is that a matched flutter Mach number is directly obtained from the damping vs a Mach graph. From the damping vs Mach graph shown in Fig. 8, a matched flutter Mach number of 0.7 is indicated. As summarized in Table 2, the results of both models are virtually the same. The slightly lower LCO onset Mach number from the flight test is already explained by the lower flutter airspeed due to the altitude difference.

Extended Model Formulation

To now, we have considered LFT models with single parameter variations in the dynamic pressure and the Mach number. When taking into account multiple simultaneous variations of the structural parameters, we speak about robust flutter analysis. Robust flutter analysis has been performed on LFT models that all have been obtained numerically. The robust LFT models are developed to reflect simultaneous uncertainties with respect to mass, damping, and stiffness. All subsequent robust LFT models have the Mach number as a varying parameter. The so-obtained flight flutter margins are robust Mach matched-point solutions. The numerical effort requested for the LFT generation led to computation times of about one-half an hour on a Pentium 700-MHz, computer.

Mass Perturbation

As experienced during flight tests, the fuel content of the pylon tank substantially influences the LCO behavior of the wing tip. To account for this effect in our analysis, we consider the pylon tank mass as a varying parameter. We define the mass perturbation M as $1/M = 1/(M_0 + \delta M)$ because, in Eqs. (7) and (15), the mass parameter enters the second row of the state-space system in an inverse manner.

The fuel tank contents can be altered from full (2600 lb per tank) down to empty in two intermediate steps, that is, between half-full and quarter-full. The wing pylon fuel tank contains three fuel compartments that are drained in sequence. The fuel state in the wing pylon fuel tank is divided into four sequences, FFF, FEF, FEE, and EEE. The fuel sequences cause irregular pylon tank center of gravity position shifts, leading to nonlinear changes in the moment of inertia of the wing. In the development of the LFT model, these effects have been taken into account. Next we performed a flutter analysis over all of the perturbed fuel states of the wing pylon fuel tank using the mass perturbed Mach parameterized LFT model. The robust analysis was performed around nominal Mach number of 0.6. The perturbation increments in the Mach number were taken to be 0.1, and the overall mass LFT model was fitted as function of Mach between Mach 0.4 and 0.9. The results of the analysis are presented in Fig. 9. These reflect the Mach flutter speed as a function of the total mass perturbation in the wing pylon fuel tank from FFF down to EEE. Analysis reveals first a decrease of the flutter speed from the fuel state FFF to FEF. Then there is again an increase of the Mach flutter speed with decreasing fuel in the wing pylon fuel tank. This is the case in both ranges where the fuel state FEF changes to FEE and from FEE to EEE. The matched Mach flutter solutions deviate at larger perturbations in the fuel state. The largest deviation Mach flutter speed was in the third perturbation run, and predictions errors did not exceed 5%. The third run led to a 500 lb perturbation result from the FEE fuel state. The last two obtained perturbations of 600 and 700 lb corresponded to flutter speeds above Mach 0.9 for both methods. These solutions were considered not to be valid because both models were fitted as a function of Mach from 0.4 up to 0.9. Frequency and damping curves of the P Mach matched method (not shown) have been generated as a function of Mach number for the FFF to EEE fuel state. In the FFF fuel state, the aeroelastic instability of the wing first bending and torsion mode reveals classical flutter behavior because the torsion mode becomes unstable at a Mach number of 0.7. In the FEF fuel state, the torsion mode becomes unstable at a Mach number of 0.58, but the damping curve crosses (not shown) the zero damping axis at a very shallow angle. The damping of the torsion mode decreases very slowly, indicating that the aeroelastic problem is not violent. The frequency and damping curves of the FEE fuel state show a similar behavior as in the FEF fuel state. With empty wing pylon fuel tanks EEE, the damping of the bending and torsion modes remain positive up to a Mach number of 0.9, which is beyond the validity region of the model. The perturbation of the fuel contents of the wing pylon tank (PT) was performed in three separate runs due to the irregularities in the fuel drainage scheme. The flutter solutions obtained using the LFT model show good correlation with the predictions from the Mach matched P method. The maximum deviation in the analysis results between the robust LFT model and the P method is 7%. To limit the difference between both solution techniques, the actual mass perturbation was constrained. How much this limitation should be is difficult to say because the difference is nonlinearly distributed with increasing mass perturbation. However, based on the total mass perturbation in Fig. 9 and a maximum difference of 5% between the solutions, the maximum perturbation should be not more than

1000 lb around the FFF fuel state. For the FEF and FEE fuel states, there are no limits for the mass perturbation because the difference between the methods never exceeded 5%. These theoretical mass perturbation limits are not considered as problematic because they are way beyond the practical mass perturbation limit. The practical limit is related to the accuracy of the aircraft weight calculation and the error in the PT fuel state determination. Based on these considerations, practical PT mass perturbation limits of ±200 lb were established. This practical perturbation limit of ±200 lb shows to have the highest effects in the third perturbation run, from FEE to EEE, where it creates a variation of the flutter Mach number of 31%.

Validation of the Robust LFT Model Using Flight-Test Results

The flight-test data consist of a collection of relevant parameters, recorded during a level acceleration at a selected altitude. The flutter analysis was performed at sea level, where the dynamic pressure is the highest possible leading to the worst-case flutter solution. Level acceleration at sea level in practice is not possible due to restrictions; however, a level acceleration at 1000-ft AGL is an admissible deviation. The data that are available are from runs above the North Sea with different fuel states. Figures 10 and 11 show time histories of flight-test results from level accelerations. From top to bottom, we have the normal acceleration of the forward and the aft station of the left wing tip a_{z1f}, a_{z1a} in ms^{-2} the normal acceleration of the forward and aft station of the right wing tip a_{z9f}, a_{z9a}, and finally the Mach number Ma as function of time. The runs are started from 250 KCAS up to the maximum operating speed V_{mo}. During the run, the altitude is closely maintained with a margin of 50 ft. Also, the fuel state of the wing pylon fuel tank was frozen by selecting internal fuel feed. With this selection, fuel is used from the internal tanks instead of fuel from the external tanks. This was done to avoid a variable fuel state in the wing pylon fuel tanks, which might influence the quality of the measurements. Figures 10 and 11 show the emerging vibration of the wing tips, which stabilize at about 20 ms^{-2} for the forward wing tip stations. The LCO starts to show up at 16 s into the run, and vibrations of the wing tips emerge at a Mach number of 0.61. Similarly, from Fig. 11, an LCO onset speed of Mach 0.57 is indicated. The acceleration data of the wing tips indicate that the forward and aft stations are 180 deg out-of-phase (i.e., left forward station goes up, while left aft station goes down), that is, the motion of the wing tips is mainly torsional. Data analysis also shows that both forward stations are 180 deg out-of-phase (i.e., left wing tip goes up, while the right wing tip goes down), that is, the motion is antisymmetric. Figure 12 shows a Fourier analysis of the measured acceleration signals. From Fig. 12, it can be seen that starting from the first fuel state the power spectral density peaks below 5 Hz, which corresponds to an LCO condition of the first wing bending mode. From the second fuel state, the power spectral density has its peak above 5 Hz, indicating that the aeroelastic instability is the antisymmetric wing torsion mode with a frequency of about 5.35 Hz.

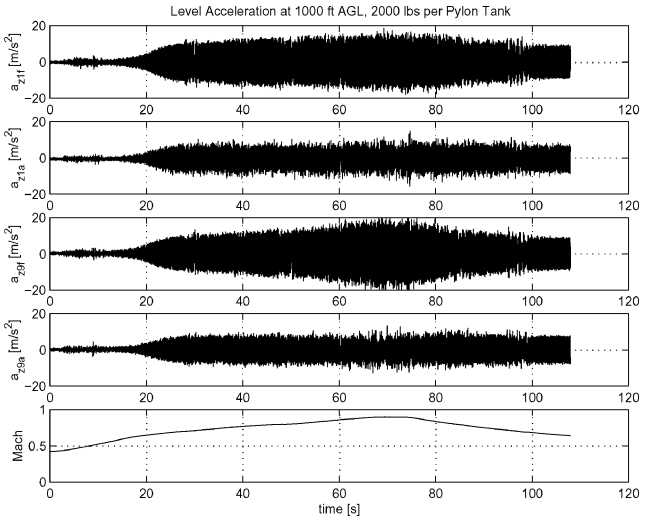

Fig. 10 Flight-test run at 1000 lb.

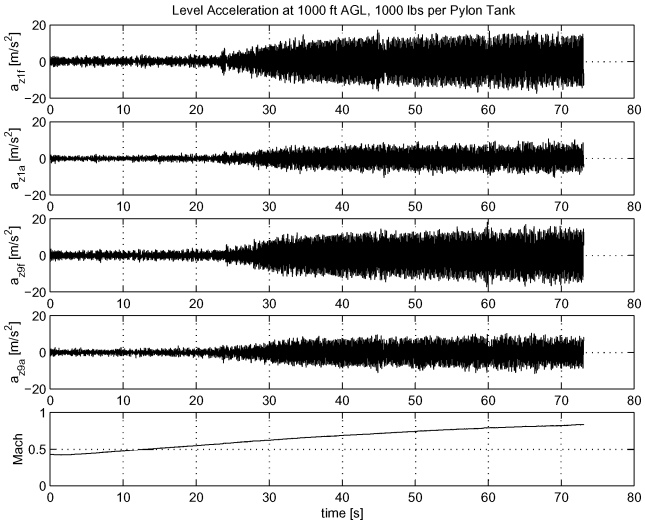

Fig. 11 Flight-test run at 2000 lb.

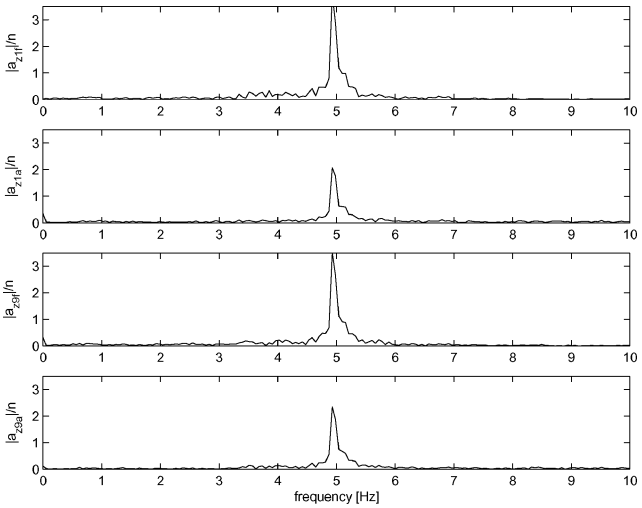

a) Power spectral analysis 2000 lb

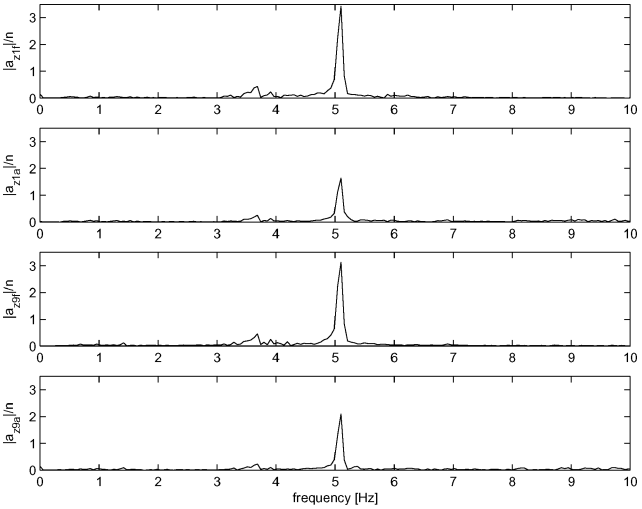

b) Power spectral analysis 1000 lb

Fig. 12 Power spectral analysis accelerations signals, level acceleration at 1000 ft AGL.

Table 3 Robustness analysis and flight tests

	Fuel state, lb/tank			
Parameter	2000	2000	1000	1000
Mass perturbation FFF, lb	400	800	1400	1800
Damp perturbation, %	0.03	0	0	0.03
Stiffness perturbation, %	+10	−10	−10	+10
Ma_{flutter}	0.79	0.6	0.57	0.85

Discussion

The LCO onset Mach numbers are compared with the flutter Mach numbers from the robust models. To establish the lowest and the highest possible flutter Mach number for the associated configuration, we assume that the fuel state of the wing pylon fuel tanks can be determined with an accuracy of ±200 lb. The first run was executed with 2000 lb per wing pylon fuel tank. This is a perturbation of 600 lb from the full fuel state FFF. With the uncertainty of ±200 lb, we have a total range of 400–800 lb perturbation from the full fuel state FFF. Similarly for the second run, which was executed with 1000 lb per wing pylon fuel tank, we establish a total range of 1400–1800 lb perturbation from the full fuel state FFF. Studying damping variation shows that the lowest flutter Mach number is at zero structural damping variation, whereas the highest flutter Mach number is at 0.03 structural damping deviation. Stiffness perturbation analysis reveals that the lowest flutter Mach number is at −10% stiffness perturbation, whereas the highest flutter Mach number is at +10% stiffness perturbation. With these perturbations, the lowest and highest possible flutter Mach number were calculated using the robust LFT model. The results of this robustness analysis are summarized in Table 3. The results from the robustness analysis shown in Table 3 indicate, for the first run, with a fuel state of 2000 lb per wing pylon fuel tank, a robust flutter Mach number between 0.6 and 0.79. From flight test data, the LCO onset Mach number was 0.61, which matches the robust flutter margin prediction. Similarly, for the second run, with a fuel state of 1000 lb per wing pylon fuel tank, the robustness analysis results indicate a flutter Mach number between 0.57 and 0.85. From flight-test data, the LCO onset Mach number was 0.57, which again matches the robust flutter margin calculations. The comparison between robustness analysis and flight-test data results indicate that the nominal models are too optimistic as far as the flutter Mach number is concerned. When perturbations in mass, damping, and stiffness are taken into account, a more realistic margin of a flutter Mach number is produced. The robustness analysis may also explain the deviation in LCO onset Mach number between different airframes. Aeroelastic analysis indicated an instability of the wing torsion mode. This mode was also confirmed by spectral and phase analysis of the flight-test data.

Conclusions

Several aeroelastic LFT model formulations have been presented for the determination of critical flutter speeds. Comparison with classical flutter analyses and flight-test data show good correlation, validating the so developed models. The LFT models parameterized in terms of the Mach number lead in a natural way to match-point flutter solutions and correlate well with flight-test data. We were able to understand the physical mechanisms behind erratic LCO behavior of the F-16A/B in heavy store configuration through the development and analysis of the Mach parameterized LFT model extended with the effect of the change in mass due to PT fuel consumption. It has been shown how the extended LFT model captures the nonlinear behavior in flutter speeds as a function of the fuel state. The effects of uncertainties in wing stiffness and damping are also taken into account and the results have permitted the establishment of a clear picture of the overall LCO behavior of the system in heavy store configuration.

Acknowledgments

The authors would like to thank R. Lind and M. Brenner from NASA Dryden Flight Research Center for their support and crucial guidance toward the development of meaningful aeroelastic linear fractional transformation (LFT) models. Furthermore, we would like to thank the group of H. Koolstra from the Royal Netherlands Air Force and the Aeroelasticity group from the Dutch National Aerospace Laboratory NLR for providing the flight-test data and the aeroelastic math models. Finally, many thanks go out to Jean-Francois Magni from ONERA and Jean-Paul Dijkgraaf from EADS for the support in the setup of the numerical LFT modeling using the linear fractional representation LFR Toolbox.

References

[1]Brenner, M., Lind, R., and Voracek, D., "Overview of Recent Flight Flutter Testing Research at NASA Dryden," AIAA Paper 97-1023, April 1997.

[2]Brenner, M., "Aeroservoelastic Modeling and Validation of a Thrust-Vectoring F/A-18 Aircraft," NASA TP-3647, Sept. 1996.

[3]Lind, R., and Brenner, M., *Robust Aeroservoelastic Stability Analysis*, Advances in Industrial Control, Springer, London, 1999.

[4]Lind, R., and Brenner, M., "Robust Flutter Margins of an F/A-18 Aircraft from Aeroelastic Flight Data," *Journal of Guidance, Control and Dynamics*, Vol. 20, No. 3, 1997, pp. 597–604.

[5]Lind, R., and Brenner, M., "Incorporating Flight Data into a Robust Aeroelastic Model," *Journal of Aircraft*, Vol. 35, No. 3, 1998, pp. 470–477.

[6]Lind, R., and Brenner, M., "Utilizing Flight Data to Update Aeroelastic Stability Estimates," AIAA Paper 97-3714, Aug. 1997.

[7]Lind, R., and Brenner, M., "A Worst-Case Approach for On-Line Flutter Prediction," *International Forum on Aeroelasticity and Structural Dynamics*, Vol. 2, 1997, pp. 79–86.

[8]Lind, R., and Brenner, M., "Worst-Case Flutter Margins from F/A-18 Aircraft Aeroelastic Data," *AIAA Structures, Structural Dynamics and Materials Conference*, AIAA, Reston, VA, 1997, pp. 738–748.

[9]Lind, R., Brenner, M., and Freudinger, L., "Improved Flight Test Procedures for Flutter Clearance," *International Forum on Aeroelasticity and Structural Dynamics*, Vol. 3, 1997, pp. 291–298.

[10]Bisplinghoff, R., Ashley, H., and Halfman, R., *Aeroelasticity*, Addison-Wesley, Cambridge, MA, 1955.

[11]Kehoe, M., "A Historical Overview of Flight Flutter Testing," *Proceedings of the 80th AGARD Structures and Materials Panel*, CP-566, AGARD, 1995, pp. 1–15.

[12]Roger, K., "Airplane Math Modeling Methods for Active Control Design," *Proceedings of the 44th AGARD Structures and Materials Panel*, CP-228, AGARD, 1977, pp. 4.1–4.11.

[13]Cooper, J., Desforges, M., Emmett, P., and Wright, J., "Advances in the Analysis of Flight Flutter Test Data," *Proceedings of the 80th AGARD Structures and Materials Panel*, CP-566, AGARD, 1995, pp. 13:1–13:12.

[14]Cooper, J., and Noll, T., "Technical Evaluation Report on the 1995 Specialists Meeting on Advanced Aeroservoelastic Testing and Data Analysis," *Proceedings of the 80th AGARD Structures and Materials Panel*, CP-566, AGARD, 1995, pp. T1–T10.

[15]Hassig, H., "An Approximate True Damping Solution of the Flutter Equation by Determinant Iteration," *Journal of Aircraft*, Vol. 8, No. 11, 1971, pp. 885–889.

[16]Chavez, F. R., "Characterizing Model Variation for Robust Control of Flexible Atmospheric Flight Vehicles," Ph.D. Dissertation, Dept. of Aerospace Engineering, Univ. of Maryland, Aug. 2000.

[17]Bécus, G., "Automated Search for the Most Critical Flutter Configuration in Models with Uncertainty," *Mathematical and Computer Modelling*, Vol. 14, 1990, pp. 977–982.

[18]Bécus, G., and Rekow, C., "Robust Control Theory Methods in Flutter Analysis," *International Forum on Aeroelasticity and Structural Dynamics*, 1991, pp. 464–468.

[19]Bécus, G., "Stability Robustness of Aeroelastic Systems: A Perturbation Approach," *International Forum on Aeroelasticity and Structural Dynamics*, Vol. 2, 1997, pp. 425–532.

[20]Lind, R., Freudinger, L., and Voracek, D., "A Comparison of Aeroelastic Excitation Mechanisms," *Journal of Aircraft*, Vol. 35, No. 5, 1998, pp. 830–832.

[21]Brenner, M., and Lind, R., "Wavelet Filtering to Reduce Conservatism in Aeroservoelastic Robust Stability Margins," AIAA Structures, Structural Dynamics, and Materials Conf., April 1998.

[22]Brenner, M., and Lind, R., "On-Line Aeroelastic Robust Stability Prediction Using Wavelet Filtering," *21st Congress of the International Council of Aeronautical Sciences*, Sept. 1998.

[23]Lind, R., Snyder, K., and Brenner, M., "Wavelet Analysis of Aeroelastic Systems with Structural Nonlinearities," *AIAA Structures, Structural Dynamics and Materials Conference*, April 1998.

[24]Lind, R., Balas, G., and Packard, A., "Robustness Analysis with Linear Time-Invariant and Time-Varying Real Uncertainty," *AIAA Guidance, Navigation and Control Conference*, AIAA, Washington, DC, 1995, pp. 132–140.

[25]Packard, A., and Doyle, J. C., "The Complex Structured Singular Value," *Automatica*, Vol. 29, No. 1, 1993, pp. 71–109.

[26]Balas, G. J., Doyle, J. C., Glover, K., Packard, A. K., and Smith, R., "μ-Analysis and Synthesis Toolbox," Math Works, Inc., 1st ed., July 1993.

[27]Fielding, C., Varga, A., Bennani, S., and Selier, M., *Advanced Techniques for Clearance of Flight Control Laws,* LNCIS 284, Springer-Verlag, Berlin, 2002.

[28]Magni, J. F., "Linear Fractional Representations: a Toolbox for Use with MATLAB," July 2001.

[29]Lambrechts, P., Terlouw, J., Bennani, S., and Steinbuch, M., *Parametric Uncertainty Modeling Using LFT's*, *Proceedings of the American Control Conference*, 1993, pp. 267–272.

[30]Belcastro, C. M., et al., "On the Validation of Safety Critical Aircraft Systems, Part I: An Overview of Analytical and Simulation Methods," *AIAA Guidance, Navigation, and Control Conference*, 2003.

[31]Belcastro, C. M., et al., "On the Validation of Safety Critical Aircraft Systems, Part II: An Overview of Experimental Methods," *AIAA Guidance, Navigation, and Control Conference*, 2003.

[32]Lind, R., "Match-Point Solutions for Robust Flutter Analysis," *Journal of Aircraft*, Vol. 39, No. 1, 2002.

[33]Beuker, B., Bennani, S., van Staveren, J. W., and Meijer, J., "Robust Flutter Analysis of an F-16A/B in Heavy Store Configuration," AIAA Paper 2002-3967, Aug. 2002.

[34]Bennani, S., Beuker, B., van Staveren, J. W., and Dijkgraaf, J.-P., "Numeric LFT Generation for Robust Aircraft Flutter Analysis," *Proceedings 2002 IEEE International Symposium on Computer Aided Control System Design*, 2002, pp. 260–265.

[35]Elrod, J., and Bensinger, C., "F-16 Flutter Analysis, Resequenced External Tank," General Dynamics, Contract Rept 16 PR 413-adl.

[36]Johnson, E. H., Nagendra, G. P., and Reymond, M. A., "Addition of Aeroelasticity to the MCS/NASTRAN Multidisciplinary Analysis and Design Capability," MacNeal-Schwendler Corp. (Technical Rept.) Los Angeles, Sept. 1991.

[37]Rodden, W. P., Taylor, P. F., and McIntosh, S. C., "Improvements to the Doublet-Lattice Method in MCS/NASTRAN," MacNeal–Schwendler Corp., Technical Rept., Los Angeles, Sept. 1999.

[38]Vepa, R., "On the Use of Padé Approximants to Represent Unsteady Aerodynamic Loads for Arbitrarily Small Motions of Wings," AIAA Paper 76-17, Jan. 1976.

[39]Abel, "An Analytical Technique for Predicting the Characteristics of a Flexible Wing Equipped with an Active Flutter-Suppression System and Comparison with Wind-Tunnel Data," NASA TP-1367, 1979.